AIAA JOURNAL
Vol. 45, No. 6, June 2007

Adaptive Feedback Optimal Control of Flow Separation on Stators by Air Injection

Nhan T. Nguyen*
NASA Ames Research Center, Moffett Field, California 94035
and
Michelle M. Bright† and Dennis Culley‡
NASA Glenn Research Center, Cleveland, Ohio 44135

DOI: 10.2514/1.18226

This paper presents an adaptive flow control approach for controlling flow separation in a stator cascade within a low-speed axial-flow compressor using an air injection technique. Flow separation usually manifests itself as an increase in a total pressure loss across a blade row. A 1-D unsteady flow model based on the Euler equations incorporating a pressure loss parameter is used to design a feedback control of the total pressure at the outlet. The feedback adaptive control strategy relies on a recursive least-square parameter estimation to estimate the effectiveness of air injection. A nonlinear trajectory optimization is developed to determine an optimal air injection gain schedule. Disturbances due to variations in the inlet flow condition at the stator blade row are minimized by a quasi-steady state error-correction feedback optimal control to maintain a desired air injection value. The nonlinear optimization and quasi-steady state feedback optimal control are recently developed based on an adjoint method for the Euler equations. A numerical simulation demonstrates the effectiveness of the proposed flow control strategy.

Nomenclature

$\mathbf{A}$	=	characteristic matrix, state transition matrix
A	=	flow passage area
a	=	coefficient of linearized Euler equation
$\mathbf{B}$	=	source vector in nonconservation form, control influence matrix
$\mathbf{C}$	=	disturbance influence matrix
c	=	speed of sound, blade chord
D	=	diffusion factor
$\mathbf{E}$	=	filter vector
e	=	internal energy
$\mathbf{F}$	=	flux vector function, boundary condition matrix
$\mathbf{G}$	=	initial flow condition
H_1	=	Hamiltonian function
H_2	=	wake form factor, Hamiltonian function
i_0	=	reference incidence angle
J	=	cost function
K	=	feedback gain
L	=	flow passage length
M	=	Mach number
m	=	Carter's rule correlation parameter
$\dot{m}$	=	mass flow
n	=	numbers of blades, Carter's rule correlation parameter
P	=	linear weighting factor of adjoint solution
p	=	pressure
p_0	=	total pressure
$\mathbf{Q}$	=	source vector in conservation form, state weighting matrix
Q	=	state weighting factor
$\mathbf{R}$	=	control weighting matrix
R	=	control weighting factor
S	=	linear weighting factor of solution of linearized Euler equation
T	=	temperature
T_0	=	total temperature
t	=	time
t_f	=	final time
$\mathbf{U}$	=	flow vector in conservation form
u	=	control variable, flow speed
$\mathbf{V}$	=	Riccati equation matrix
V	=	velocity
$\mathbf{v}$	=	disturbance vector
v	=	air injection mass flow
$\mathbf{W}$	=	Riccati equation matrix
$\mathbf{x}$	=	state vector
x	=	flow passage curvilinear coordinate
$\mathbf{y}$	=	flow variables in nonconservation form
β	=	air angle
γ	=	specific heat ratio
δ_0^0	=	reference deviation angle
$\boldsymbol{\eta}$	=	boundary adjoint vector
θ	=	blade camber angle, angular coordinate in tangential direction
θ^*	=	wake momentum thickness
$\boldsymbol{\lambda}$	=	distributed adjoint vector
λ	=	distributed adjoint vector
ξ	=	total pressure loss parameter
ρ	=	density
σ	=	blade solidity
$\bar{\omega}$	=	total pressure loss coefficient

Prefixes

Δ	=	difference, error
δ	=	variation

Subscripts

0	=	stagnation condition
1	=	inlet condition
2	=	outlet condition

Presented as Paper 6072 at the AIAA Guidance, Navigation, and Control Conference, San Francisco, CA, 15–18 August 2005; received 3 August 2005; accepted for publication 18 November 2006.

*Research Scientist, Intelligent Systems Division, Mail Stop 269-1.
†Research Engineer, Control and Dynamics Technology Branch, Mail Stop 77-1.
‡Research Engineer, Control and Dynamics Technology Branch, Mail Stop 77-1.

Superscript

T = matrix transpose operation

I. Introduction

AN AIRCRAFT gas turbine engine comprises several major aeromechanical components including compressors, combustors, and turbines. Within a compressor stage, stator and rotor cascades provide alternate flow passages through which a diffusion process takes place that results in an increase in the static pressure. Under critical operating conditions such as those during takeoff and landing, mass flow deficit or inlet distortion may result. As a consequence, the incidence angle on the blade row may increase substantially beyond an acceptable limit, thus causing stall and flow separation. Current research in flow control in gas turbine engines attempts to improve the design and operation of compressors by flow control augmentation methods. This may potentially result in a more efficient operation or a potentially new compressor design with fewer stages [1]. The benefits of improved efficiency in future gas turbine engines using flow control technologies would lead to a lower fuel consumption and reduced harmful NOx emissions in the atmosphere.

Compressor flow control methods have been investigated by many researchers and there exists a large body of knowledge pertaining to this area of research [2–4]. Recently, a fluid injection flow control concept has been developed at NASA Glenn Research Center to control flow separation in a stator cascade [5]. Highly specialized flow control vanes are fabricated to incorporate a series of air injection slots on the suction surface as shown in Fig. 1.

The air injection coverage is from approximately 10–90% of span and is constrained by the vane cavity design. The flow control vanes produce steady injection or unsteady injection when coupled with an external flow modulating valve. The optimum injection location on the suction surface is 35% of the chord as determined in a wind-tunnel study performed by the Illinois Institute of Technology [5]. In all vane configurations, the injection angle is pitched at 30 deg relative to the vane upper surface to impart a streamwise momentum to the flow. The working principle of the air injection flow control is based on the well-known boundary layer physics which shows that the boundary layer growth can usually be attenuated by a high momentum small-scale flow, which helps energize the low momentum air accumulated near the blade suction surface by promoting fluid momentum exchange. Experimental testing in the low speed axial-flow compressor (LSAC) test facility at NASA Glenn Research Center has demonstrated that this flow control method is effective in reducing a flow blockage caused by a boundary layer growth formed within a stator cascade [5]. The current flow control concept is an open-loop implementation without any feedback. This study will address the feedback design for this flow control concept.

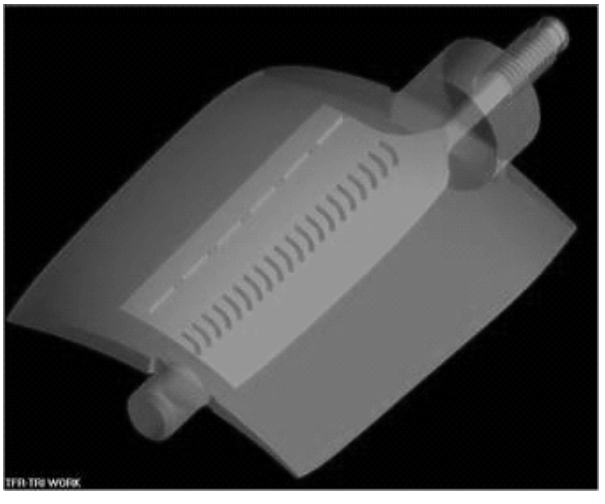

Fig. 1 Flow control stator vane.

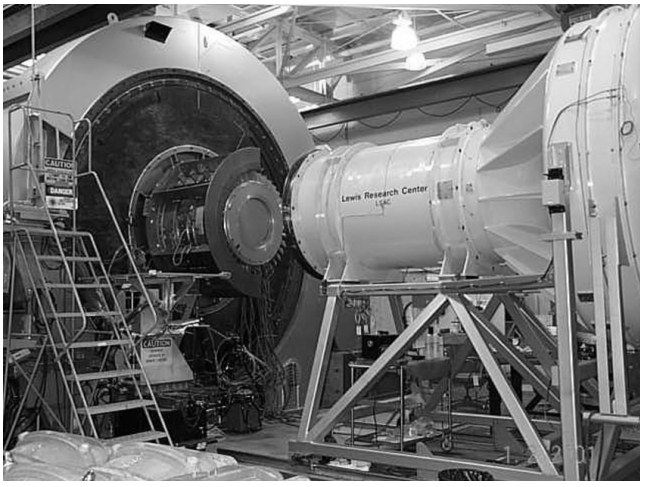

Fig. 2 NASA Glenn low-speed axial-flow compressor (LSAC) test facility.

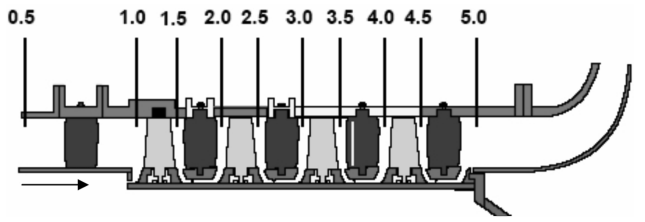

Fig. 3 Compressor stages.

Figure 2 shows the LSAC test facility. The LSAC compressor is driven by a 1500-hp variable speed motor and consists of an inlet guide vane and four identical stages designed for accurate low-speed simulation of the rear stages of a high-speed core compressor. With reference to Fig. 3, the first two stages are used to set up a repeating stage environment. The third stage is the focus of research measurements, while the fourth stage acts as a buffer to the exit conditions. The flow path has an outer diameter of 1.219 m and a hub-tip radius ratio of 0.80. The nominal rotor tip and stator seal clearances are 1.4 and 0.6% of span, respectively. Rotor tip speed is 61 m/s and nominal axial velocity is on the order of 25 m/s. The flow control stator vanes located in the third stage are designed by applying modified NACA 65-series thickness distributions to modified circular-arc mean lines.

To implement this flow control technology in future gas turbine engines, an effective feedback control strategy must be employed. Moreover, the flow control strategy must be capable of a real-time execution in a gas turbine engine operating environment. A prevailing method in the flow control research is based on the Moore–Greitzer model [6], which is widely used to study stall control. This model is a three-state model for a compression system based on a single mode Galerkin projection. The problem with the Moore–Greitzer model is that it is based on a reduced parametric model of compressor stall dynamics whose parameters are difficult to estimate due to highly complex stall flow. Furthermore, the Moore–Greitzer model is based on incompressible flow and does not address the intermediate flow along a compressor cascade. In this paper, we present a feedback adaptive flow control design using a physics-based distributed model coupled with a parameter estimation for a flow control design purpose. The distributed model is formulated using the 1-D unsteady Euler equations of motion for compressible flow that can have a wide range of applicability beyond the immediate flow control problem in a compressor cascade. A loss parameter is incorporated into the Euler equations to represent the effect of the total pressure loss due to flow separation. An adjoint-based optimal control theory for the 1-D Euler model is developed for the flow control approach.

II. Diffusion Concept

In diffusing flow, stall often occurs due to the presence of an adverse pressure gradient. Stall flow usually manifests itself as a reduced static pressure recovery and an increase in the total pressure loss [7]. Thus, the total pressure loss can be seen as an indicator for stall or flow separation. Lieblein showed that the stall onset relates to a parameter known as a diffusion factor which is well correlated with the boundary layer wake momentum thickness in the minimum-loss region of a 2-D compressor cascade [8]. A local diffusion factor D_{loc} is defined as the ratio of the velocity difference between the maximum velocity $V_{\max}$ and the outlet velocity V_2 to the maximum velocity on the suction surface

$$D_{\text{loc}} = \frac{V_{\max} - V_2}{V_{\max}} \tag{1}$$

Typically, a detailed knowledge of the velocity distribution on a compressor blade section is usually not known, so Lieblein alternatively defined a more convenient form of the diffusion factor based on the inlet and outlet velocities of the cascade according to

$$D = \left(1 - \frac{V_2}{V_1}\right) + \frac{\Delta V_\theta}{2\sigma V_1} \tag{2}$$

where ΔV_θ is the change in the tangential velocity through the cascade.

For an incompressible 2-D cascade, Eq. (2) becomes

$$D = \left(1 - \frac{\cos\beta_1}{\cos\beta_2}\right) + \frac{\cos\beta_1}{2\sigma}(\tan\beta_1 - \tan\beta_2) \tag{3}$$

A theoretical analysis of incompressible 2-D cascade total pressure loss [8] shows that the momentum thickness θ^* correlates well with the total pressure loss coefficient $\bar{\omega}_1$ based on the inlet condition according to the relationship

$$\bar{\omega}_1 = \frac{p_{0,1} - p_{0,2}}{p_{0,1} - p_1} = 2\left(\frac{\theta^*}{c}\right)_2 \frac{\sigma}{\cos\beta_2}\left(\frac{\cos\beta_1}{\cos\beta_2}\right)^2 \left\{\frac{\frac{2H_2}{3H_2 - 1}}{\left[1 - \left(\frac{\theta^*}{c}\right)_2 \frac{\sigma H_2}{\cos\beta_2}\right]^3}\right\} \tag{4}$$

Hence, an increase in the wake momentum thickness resulting from flow separation in the cascade directly translates into an accompanied increase in the total pressure loss. Figure 4 obtained from the NASA SP-36 report [8] illustrates the diffusion factor correlation for a NACA 65-(A_{10})10 low-speed compressor cascade.

As illustrated in Fig. 4, the diffusion factor is correlated well with the total pressure loss coefficient as defined in Eq. (4). Lieblein showed that the total pressure loss coefficient is generally a reliable indicator of the momentum thickness of the boundary layer formed over the blade surface. Thus, the larger the total pressure loss coefficient, the thicker the boundary layer becomes. It is generally accepted that stall onset occurs at about a diffusion factor of 0.55 or above where the total pressure loss begins to increase rapidly [8] due to the thickening of the boundary layer, as can be seen in Fig. 4.

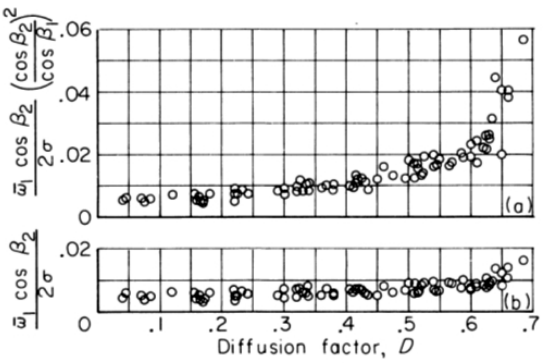

Fig. 4 Diffusion factor correlation.

Based on the diffusion concept, it is reasonable to say that controlling flow separation is tantamount to controlling the total pressure loss. The most direct effect of this total pressure loss control is an increase in the static pressure recovery in a diffusing flow through the stator cascade. More important, this control also brings about a reduction in the boundary layer thickness, which therefore increases the turning angle and hence decreases the angle of attack on the rotor blade row to alleviate the stall flow on the rotor.

Thus, in a compressor environment, the total pressure measurement across a blade row can provide an indication of the potential stall onset. Typically, designers should know the design total pressure loss across a blade row, which could also be measured directly by running the compressor at the design point. When operating substantially above this design value, for example, twice the design loss, an inference could be made about a probable flow separation event in the compressor that needs to be corrected. Flow control vanes can then be activated to inject bleed air into the flow passage to bring about a reduction in the total pressure loss.

III. Adaptive Flow Control Architecture

In this study, a model-based flow control approach is proposed for controlling the total pressure loss across a stator cascade equipped with flow control vanes. The flow control architecture incorporates an adaptive parameter estimation that can estimate online the relationship between the air injection mass flow and the total pressure loss under a varying engine operating environment. To minimize errors in the parameter estimation during the initial phase of estimation, computational fluid dynamics (CFD) modeling will be used to provide data for an off-line estimation. Although CFD technologies have been advancing rapidly in many facets of fluid dynamics applications including turbomachinery, the complex nature of flow separation still poses a significant challenge in estimating total pressure losses in a compressor cascade using CFD modeling alone. Nonetheless, CFD modeling can greatly complement the limited knowledge obtained from experimentation to provide a better understanding of the flow characteristics. An effective flow control architecture therefore should incorporate both CFD modeling as well as experimental data in its design by leveraging the complementary nature of analytical and experimental methods.

Realizing that the flow environment in a compressor stage within a gas turbine engine can be quite complex, any flow control concept cannot possibly address all the subtlety of the real flow details in an actual gas turbine engine. Therefore, although the proposed flow control concept based on the 1-D Euler model may appear to overly simplify the real flow inside a compressor cascade, the incorporation of the parameter estimation into the flow control architecture is designed to complement the analytical model with real data from the gas turbine engine as an attempt to address the real flow problem. This approach is equivalent to the design process of a compressor which traditionally can be performed with simplified mathematical modeling combined with cascade empirical correlations to accurately estimate the velocity distribution within the cascade.

The road map for this fundamental research is to initially develop the proposed flow control concept that can be implemented in the LSAC test facility for demonstration of its feasibility. While the LSAC compressor is a low-speed compressor, it shares a number of similar features with the low-pressure compressor spool in a modern gas turbine engine, including a high hub-to-tip ratio and a high blade loading design, that make it a suitable flow control research environment for gas turbine engines. This would potentially facilitate the technology transition into gas turbine engines at the end of the research phase.

Figure 5 illustrates a simplified block diagram of a flow control architecture which comprises three major features as follows:

1) *A recursive least-square parameter estimator* is incorporated into the flow control architecture to estimate a total pressure loss parameter that relates the air injection mass flow and the total

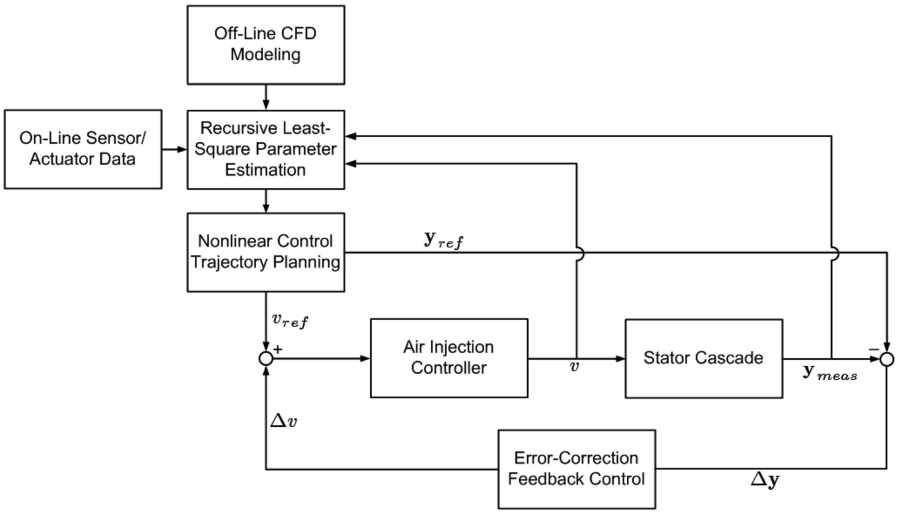

Fig. 5 Flow control architecture.

pressure loss. This parameter will then be used in the distributed model for control design purposes. The total pressure loss data are obtained from experimental testing in the LSAC test facility at NASA Glenn Research Center. Additionally, a CFD simulation is performed to provide total pressure loss data at various different air injection mass flow values and compressor configurations that were not available from experimental data. The CFD data are then used for an initial off-line estimation of the air injection control effect on the total pressure loss. This ensures that the initial air injection control is sufficiently accurate to maintain a reasonable flow control performance. During an actual engine operation, as data become available from actual pressure, temperature, and flow sensors and air injection control actuator, the recursive least-square estimator continues to improve the accuracy of the model parameter. The parameter estimation therefore allows the controller to be adaptive to different physical plant behaviors than anticipated and also to be better responsive to system uncertainties.

2) *A nonlinear trajectory optimization* is designed to provide a tracking control for maintaining a given target total pressure at the outlet of the stator cascade. The trajectory optimization is based on an adjoint method for the 1-D Euler equations with an interior pointwise control input that represents the air injection mass flow. This nonlinear optimization can be performed online based on a set point input to provide a gain schedule for the air injection mass flow.

3) *An error-correction feedback optimal control* is designed to provide a corrective control that will minimize the error signals between the model output from the nonlinear trajectory optimization and the actual measurements of the total pressure at the outlet of the stator cascade. This corrective control is necessary to correct for modeling errors and changing inlet flow conditions which can cause a deviation in the trajectory, hence an error in the target total pressure.

From the instrumentation standpoint, the flow control architecture will use pressure and temperature sensors at both the inlet and outlet to actively monitor changes in the total pressure loss parameter. When the control system detects a total pressure loss parameter increasing beyond an allowable threshold, it will dispatch a command to raise the total pressure at the outlet to a desired value so as to maintain the total pressure loss to within an acceptable limit.

IV. 1-D Curvilinear Unsteady Flow Model

Flow through a compressor cascade is generally unsteady, viscous, and three dimensional as the flowfield varies in both the meridional and tangential planes. In addition to the main flow in the inviscid core, significant secondary flowfields near the hub and tip regions may also exist. Local flowfields around blade sections resulting from a potential effect at the leading edge and wake effect at the trailing edge create tangential variations in the global flowfield. Turbomachinery flow therefore is a very complex problem to analyze. In spite of the complexity, traditional compressor design methodologies often rely on simplified analyses that address the dominant features of the flowfield. Secondary effects such as boundary layer blockage, tip clearance flow, and viscous losses are addressed in the design processes by simplified analytical and/or empirical methods. One such simplification is to ignore the flowfield tangential variation in the bladeless region, thereby resulting in an axisymmetric flowfield assumption which has been frequently used in the compressor design processes [9]. The flow properties in an axisymmetric flowfield therefore can be interpreted in a circumferential average sense. Another simplification for compressors with slightly varying end wall diameters is by neglecting the radial flow effect.

In the current flow control concept, the air injection slots admit equal mass flow that depends on sensing at a particular radial station along the flow control vanes such as the tip radius where the viscous loss is most severe. Pressure loss information at this blade station is then used in the control design for the air injection. Thus, for this application, we can restrict the flowfield on a cylindrical surface by neglecting the radial flowfield effect. The flowfield therefore varies in the axial and tangential directions. Although this flowfield can be computed by solving the Navier–Stokes equations using CFD methods, the computational speed for even a 2-D flow is not sufficiently fast for a typical real-time demand in flow control applications. Therefore, reduced-order modeling has been frequently used in flow control applications [10] in recognition that a reduced fidelity of the flowfield modeling can be traded for an increase in the computational speed. Moreover, the detail computed 2-D flowfield around the flow control vanes would tend to provide information that cannot be directly correlated with the flow control experiment because the measured total pressure losses are usually based on their tangential average values, which are commonly used in determining a compressor cascade performance based on the diffusion factor concept.

Figure 6 illustrates a 2-D flow through a compressor cascade wherein the stagnation streamlines in effect form a curved, diffusing flow passage through the compressor cascade.

In this study, we propose a reduced-order model of this flowfield using the 1-D curvilinear unsteady flow Euler equations with a total pressure loss parameter that accounts for the viscous dissipation of a real fluid caused by flow separation. This parameter is estimated by a parameter estimation process as a function of the air injection mass flow control, so in effect this parameter provides a means to reconcile the analytical model with experimental data. The 1-D curvilinear flowfield thus represents an average flow through the cascade at any given cross section normal to the flow. For 1-D unsteady flow, the Euler equations comprising the continuity, momentum, and energy equations in the conservation form are [11]

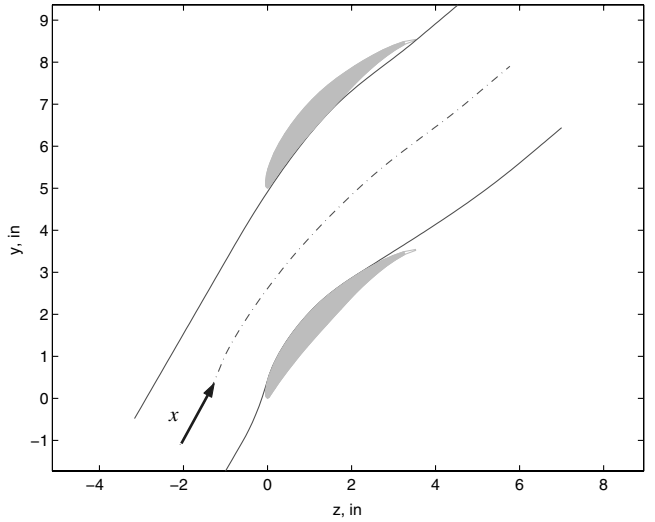

Fig. 6 Flow through a compressor cascade.

$$\mathbf{U}_t + \mathbf{F}(\mathbf{U})_x + \mathbf{Q}(\mathbf{U}, x, v) = \mathbf{0} \tag{5}$$

with

$$\mathbf{U} = \begin{bmatrix} \rho A \\ \rho u A \\ \rho A(e + \frac{1}{2}u^2) \end{bmatrix}, \qquad \mathbf{F}(\mathbf{U}) = \begin{bmatrix} \rho u A \\ \rho u^2 A + pA \\ \rho u A(e + \frac{1}{2}u^2) + puA \end{bmatrix}$$

$$\mathbf{Q}(\mathbf{U}, x, v) = \begin{bmatrix} 0 \\ -p\frac{\mathrm{d}A}{\mathrm{d}x} + \frac{1}{2}\rho u^2 A\frac{\xi(x,v)}{L} \\ 0 \end{bmatrix}$$

where $A(x)$ is the normal flow area as a function of the position x, and $\xi(x, v)$ is the total pressure loss parameter as a function of the air injection mass flow control v as well as the curvilinear coordinate x.

The function $\mathbf{F}$ is a flux function of the conserved variables, namely, mass flux, momentum flux, and energy flux. The function $\mathbf{Q}$ is a nonhomogeneous source term due to the viscous dissipation as well as the area change. For subsonic flow, the nonconservation form of the Euler equations can be used alternatively in terms of the three typical performance variables in a compressor, namely, the mass flow $\dot{m} = \rho u A$, the total pressure p_0, and the total temperature T_0 according to

$$\mathbf{y}_t + \mathbf{A}(\mathbf{y}, x)\mathbf{y}_x + \mathbf{B}(\mathbf{y}, x)\xi(x, v) = \mathbf{0} \tag{6}$$

where $\mathbf{y}(x, t) = [\,\dot{m} \quad p_0 \quad T_0\,]^T$ is a vector of flow variables and

$$\mathbf{A} = \begin{bmatrix} u & \frac{pA}{p_0} & \frac{\dot{m}u}{2T_0} \\ \frac{\rho_0 c^2}{\rho A} & u[1 - \frac{(\gamma-1)T}{T_0}] & \frac{\rho_0 c^2 u}{T_0} \\ \frac{(\gamma-1)T}{\rho A} & -\frac{(\gamma-1)^2 Tu}{kp_0} & u[1 + \frac{(\gamma-1)T}{T_0}] \end{bmatrix}$$

$$\mathbf{B} = \begin{bmatrix} \frac{\dot{m}u}{2L} \\ \frac{\rho_0 u^3}{2L}(\frac{T_0}{T} - \gamma + 1) \\ -\frac{(\gamma-1)uT}{L}(\frac{T_0}{T} - 1) \end{bmatrix}$$

where ρ_0 is the total density.

The nonconservation form of the Euler equations is more convenient and hence preferred for the adjoint analysis in this study. Equation (6) in fact also preserves the conservation of mass and energy by observing that its steady-state form is

$$\frac{\mathrm{d}\mathbf{y}}{\mathrm{d}x} = -\mathbf{A}^{-1}(\mathbf{y}, x)\mathbf{B}(\mathbf{y}, x)\xi(x, v) \Leftrightarrow \frac{d}{\mathrm{d}x}\begin{bmatrix} \dot{m} \\ p_0 \\ T_0 \end{bmatrix} = -\begin{bmatrix} 0 \\ \frac{\gamma p_0 M^2 \xi}{2L} \\ 0 \end{bmatrix} \tag{7}$$

Equation (6) is classified as a quasi-linear hyperbolic partial differential equation (PDE). The hyperbolicity comes from the fact that the eigenvalues of $\mathbf{A}$ are real and distinct. In fact, it can be shown that $\lambda(\mathbf{A}) = u,\ u \pm c$ are the eigenvalues, which are the wave propagation speeds in a fluid medium. Subsonic flow therefore involves two waves propagating downstream and one wave propagating upstream from the source. Because the flow information is propagated in both directions, data must exist at the two end point boundaries. Furthermore, the number of upstream and downstream boundary conditions must match the number of upstream and downstream wave speeds. This is known as the boundary condition compatibility. Accordingly, we need to impose appropriate boundary conditions for this flow model based on the sign definiteness of the eigenvalues. Let $x = 0$ denote the coordinate at the cascade inlet, and $x = L$ denote the coordinate at the outlet; then these boundary conditions may be specified as

$$\mathbf{F}\mathbf{y}(0, t) + (\mathbf{I} - \mathbf{F})\mathbf{y}(L, t) = \mathbf{G}(t) \tag{8}$$

where $\mathbf{I}$ is the identity matrix,

$$\mathbf{F} = \begin{bmatrix} 0 & 0 & 0 \\ 0 & 1 & 0 \\ 0 & 0 & 1 \end{bmatrix}$$

and $\mathbf{G}(t) = [\,\dot{m}_i \quad p_{0,i} \quad T_{0,i}\,]^T$ is the inlet flow condition.

Equation (8) satisfies the boundary compatibility condition. We note that the boundary condition (8) specifies that the mass flow quantities at the inlet and the outlet are the same based on the observation that the air injection mass flow is only about 1% of the total mass flow through the cascade passage. We also impose an initial condition based on the flow initially at a steady-state condition according to

$$\mathbf{y}(x, 0) = \mathbf{y}_i(x) \tag{9}$$

so that $\mathbf{y}_i(x)$ is a solution of Eq. (7) with a compatible boundary condition

$$\mathbf{F}\mathbf{y}_i(0) + (\mathbf{I} - \mathbf{F})\mathbf{y}_i(L) = \mathbf{G}(0) \tag{10}$$

Equations (6), (8), and (9) thus completely define the 1-D model of a through flow through a compressor cascade. An advantage of this 1-D model is that we can set up a flow control problem for multistage compressor cascade without requiring extensive computing resources, and it allows experimental total pressure data to be incorporated directly into the analytical model via the total pressure loss parameter. For the current research, we will use this flow control model on a single stator row.

V. Parameter Estimation

The total pressure loss parameter ξ in Eq. (6) models the total pressure loss in the compressor cascade. For air injection control, we postulate that this total pressure loss parameter is a nonnegative function of the air injection mass flow control variable v that would result in a lower total pressure loss than when the air injection is not active. Thus, we have the following equation:

$$\xi(x, v) = \xi_0(x) - \Delta\xi(x, v) \geq 0 \tag{11}$$

where ξ_0 is the baseline total pressure loss parameter without air injection control, and $\Delta\xi \geq 0$ is a total pressure loss reduction parameter due to air injection mass flow.

Using this model, controlling flow through a cascade is tantamount to controlling the total pressure loss reduction parameter via the air injection mass flow input to reduce the total pressure loss through the cascade. Generally, this total pressure loss reduction parameter is not known a priori and must be estimated as a function of the air injection mass flow. The LSAC experimental data gathered on the effectiveness of the air injection mass flow control on the total pressure loss parameter are used as a database for establishing this estimation. Based on an experimental data observation, it appears that the total pressure loss parameter varies with the air injection mass flow control according to a quadratic relationship as shown in Fig. 7. Therefore, we select a recursive least-square (RLS) approach for the

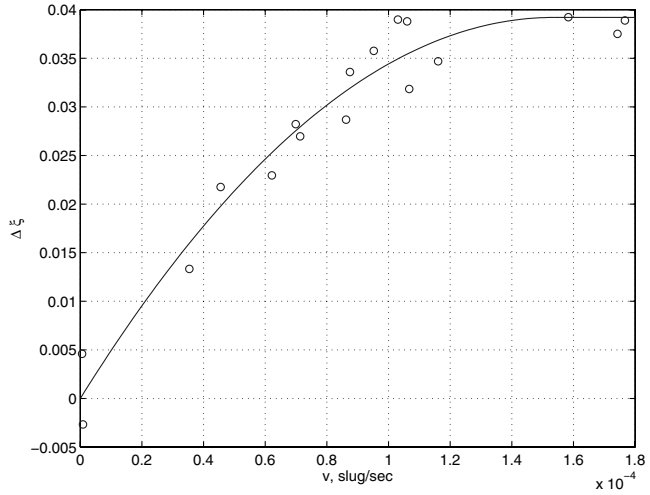

Fig. 7 Total pressure loss reduction parameter estimation.

parameter estimation. The advantage with the quadratic relationship is that the control derivative is simpler and therefore easier to implement in a nonlinear trajectory optimization process. Based on the LSAC test data, for a preliminary control design, we select the following functional form for estimating the pressure loss relationship:

$$\frac{\Delta\xi(x,v)}{\Delta\xi_{\max}} = \begin{cases} 0 & x < a, \quad \forall\ v(t) \\ \frac{v(t)}{v_{\text{sat}}}\left[2 - \frac{v(t)}{v_{\text{sat}}}\right] & x \geq a, \quad v(t) < v_{\text{sat}} \\ 1 & x \geq a, \quad v(t) \geq v_{\text{sat}} \end{cases} \tag{12}$$

where $x = a$ is the coordinate of the air injection location on the stator blade taken to be 35% of the chord, and v_{sat} is the saturation air injection mass flow taken to be about 1.54×10^{-4} slug/s or 0.86% of the total mass flow.

This model accounts for a control saturation when additional air injection beyond this value causes no further reduction in the total pressure loss. Also, the model assumes that the total pressure is unaffected upstream of the point of air injection on the stator blade. The initial estimate of the parameter $\Delta\xi_{\max}$ is computed to be 0.039 from an off-line least-square method using the LSAC test data as well as CFD data. The estimated functional relationship of the total pressure loss reduction parameter with the air injection mass flow is plotted in Fig. 7.

During an air injection flow control actuation, this parameter is continuously refined by a more efficient recursive least-square method which revises the new estimation incrementally using the results of the prior estimation. The equation of the recursive least-square method is [12]

$$\Delta\hat{\xi}_{\max,i+1} = \Delta\hat{\xi}_{\max,i} + \left(\mathbf{H}_i^T\mathbf{H}_i\right)^{-1}\mathbf{H}_{i+1}^T\left[\mathbf{H}_{i+1}\left(\mathbf{H}_i^T\mathbf{H}_i\right)^{-1}\mathbf{H}_{i+1}^T\right]^{-1} \times \left(\mathbf{z}_{i+1} + \mathbf{H}_{i+1}^T\Delta\hat{\xi}_{\max,i}\right) \tag{13}$$

where $\mathbf{z} = [\,\Delta\xi_1 \quad \Delta\xi_2 \quad \cdots \quad \Delta\xi_n\,]^T$ and

$$\mathbf{H} = \begin{bmatrix} \frac{v_1}{v_{\text{sat}}}\left(2 - \frac{v_1}{v_{\text{sat}}}\right) \\ \frac{v_2}{v_{\text{sat}}}\left(2 - \frac{v_2}{v_{\text{sat}}}\right) \\ \vdots \\ \frac{v_n}{v_{\text{sat}}}\left(2 - \frac{v_n}{v_{\text{sat}}}\right) \end{bmatrix}$$

The idea is to start out the air injection control using an initial estimate of the total pressure loss reduction parameter. A nonlinear trajectory optimization computes an initial air injection control trajectory for flow control implementation. After a predetermined n number of time steps, the computation uses the newly available total pressure loss data and the air injection mass flow input at the previous n time steps to revise the initial estimate of the total pressure loss reduction parameter using the recursive least-square method. The nonlinear trajectory optimization then uses this newly revised parameter and computes a revised air injection control trajectory. This process is then repeated for every n numbers of time steps until a desired total pressure at the outlet is achieved. A similar process can also be implemented in the error-correction feedback using the deviation of the estimated parameter.

VI. Optimal Trajectory Planning

An optimal trajectory planning is designed to compute a control gain schedule for the air injection control to achieve a total pressure set point at the outlet. Because fluid flow is governed by the nonlinear Euler equations, the trajectory planning is a nonlinear programming optimal control problem. Optimal control of distributed systems modeled by PDEs such as the Euler equations is a current subject of many mathematical researchs. In fluid problems, one approach is to transform the Euler equations into a system of ordinary differential equations (ODEs) by means of numerical discretization techniques such as finite difference methods [13] or finite element methods [14]. Discrete adjoint equations are then formulated for this discretized system. Another approach is to obtain continuous adjoint equations directly from the Euler equations via optimality conditions. This approach enjoys a considerable popularity in the aerodynamic shape optimization studies involving the Euler and Navier–Stokes equations [15]. The continuous adjoint approach is generally preferred over the discrete adjoint approach for Navier–Stokes flow problems [16]. In this study, we present a continuous adjoint method for a time-based optimization of the 1-D unsteady Euler equations. This is a significant difference from the adjoint approaches used for the aerodynamic shape optimization [15,16].

For the problem at hand, we would like to minimize the following linear-quadratic cost function with a fixed terminal time t_f subject to Eqs. (5–9):

$$J = \frac{1}{2}\int_0^{t_f}\{Q[\mathbf{y}(L,t) - \mathbf{y}_d(L)]^T\mathbf{E}^T\mathbf{E}[\mathbf{y}(L,t) - \mathbf{y}_d(L)] + R(v - v_d)^2\}\,\mathrm{d}t \tag{14}$$

where $Q \geq 0$ and $R > 0$ are some weighting factors, $\mathbf{E} = [\,0 \quad 1 \quad 0\,]$ filters out $p_0(L,t)$ from the output vector $\mathbf{y}(L,t)$ as defined in Eq. (6), the superscript T denotes a matrix transpose operation, and $\mathbf{y}_d(L)$ and $v_d \leq v_{\text{sat}}$ are the desired total pressure set point at the outlet and the corresponding air injection mass flow control computed from the steady-state Euler equations

$$\mathbf{A}(\mathbf{y}_d, x)\frac{\mathrm{d}\mathbf{y}_d}{\mathrm{d}x} + \mathbf{B}(\mathbf{y}_d, x)\xi(x, v_d) = \mathbf{0} \tag{15}$$

The necessary conditions for optimality of this system can be obtained from the variational principle. To that end, we now introduce the following dual Hamiltonian system [17]:

$$H_1(\mathbf{y}, x, v, \boldsymbol{\lambda}) = -\boldsymbol{\lambda}^T\mathbf{B}\xi(x, v) \tag{16}$$

$$H_2(\mathbf{y}(0,t),\mathbf{y}(L,t),v,\boldsymbol{\eta}) = \tfrac{1}{2}Q[\mathbf{y}(L,t) - \mathbf{y}_d(L)]^T\mathbf{E}^T\mathbf{E}[\mathbf{y}(L,t) - \mathbf{y}_d(L)] + \tfrac{1}{2}R(v - v_d)2 + \boldsymbol{\eta}^T[\mathbf{F}\mathbf{y}(0,t) + (\mathbf{I} - \mathbf{F})\mathbf{y}(L,t) - \mathbf{G}] \tag{17}$$

where $\boldsymbol{\lambda}(x,t)$ is a continuous adjoint vector for Eq. (6) and $\boldsymbol{\eta}(t)$ is an adjoint vector for the boundary condition (8).

Then the augmented cost function becomes

$$J = \int_0^{t_f}\int_0^{L}[H_1 - \boldsymbol{\lambda}^T(\mathbf{y}_t + \mathbf{A}\mathbf{y}_x)]\,\mathrm{d}x\,\mathrm{d}t + \int_0^{t_f} H_2\,\mathrm{d}t \tag{18}$$

We compute the first variation of the cost function J as

$$\delta J = \int_0^{t_f}\int_0^{L}[H_{1,\mathbf{y}}\delta\mathbf{y} + H_{1,v}\delta v - \boldsymbol{\lambda}^T(\delta\mathbf{y}_t + \mathbf{A}\delta\mathbf{y}_x + \mathbf{A}_{\mathbf{y}}\mathbf{y}_x\delta\mathbf{y})]\,\mathrm{d}x\,\mathrm{d}t + \int_0^{t_f}[H_{2,\mathbf{y}(0,t)}\delta\mathbf{y}(0,t) + H_{2,\mathbf{y}(L,t)}\delta\mathbf{y}(L,t) + H_{2,v}\delta v]\,\mathrm{d}t \tag{19}$$

Invoking Green's theorem yields

$$\iint_{\Omega}\boldsymbol{\lambda}^T(\delta\mathbf{y}_t + \mathbf{A}\delta\mathbf{y}_x + \mathbf{A}_{\mathbf{y}}\mathbf{y}_x\delta\mathbf{y})\,\mathrm{d}x\,\mathrm{d}t = -\iint_{\Omega}\left(\boldsymbol{\lambda}_t^T + \boldsymbol{\lambda}_x^T\mathbf{A} + \boldsymbol{\lambda}^T\mathbf{A}_x\right)\delta\mathbf{y}\,\mathrm{d}x\,\mathrm{d}t + b \tag{20}$$

where the boundary condition term b is computed by integrating the contour integral on the boundary Γ with zero variations of b at $x = 0$ and $t = 0$

$$b = \oint_{\Gamma}(\boldsymbol{\lambda}^T\mathbf{A}\delta\mathbf{y}dt - \boldsymbol{\lambda}^T\delta\mathbf{y}\,\mathrm{d}x) = \int_0^{t_f}[\boldsymbol{\lambda}^T(L,t)\mathbf{A}(\mathbf{y}(L,t),L)\delta\mathbf{y}(L,t) - \boldsymbol{\lambda}^T(0,t)\mathbf{A}(\mathbf{y}(0,t),0)\delta\mathbf{y}(0,t)]\,\mathrm{d}t + \int_0^{L}\boldsymbol{\lambda}^T(x,t_f)\delta\mathbf{y}(x,t_f)\,\mathrm{d}x \tag{21}$$

Using the foregoing results, the first variation of the cost function J becomes

$$\delta J = \int_0^{t_f}\int_0^{L}[(H_{1,\mathbf{y}} + \boldsymbol{\lambda}_t^T + \boldsymbol{\lambda}_x^T\mathbf{A} + \boldsymbol{\lambda}^T\mathbf{A}_x)\delta\mathbf{y} + H_{1,v}\delta v]\,\mathrm{d}x\,\mathrm{d}t - \int_0^{L}\boldsymbol{\lambda}^T(x,t_f)\delta\mathbf{y}(x,t_f)\,\mathrm{d}x - \int_0^{t_f}[\boldsymbol{\lambda}^T(L,t)\mathbf{A}(\mathbf{y}(L,t),L)\delta\mathbf{y}(L,t) - \boldsymbol{\lambda}^T(0,t)\mathbf{A}(\mathbf{y}(0,t),0)\delta\mathbf{y}(0,t)]\,\mathrm{d}t + \int_0^{t_f}[H_{2,\mathbf{y}(0,t)}\delta\mathbf{y}(0,t) + H_{2,\mathbf{y}(L,t)}\delta\mathbf{y}(L,t) + H_{2,v\delta v}]\,\mathrm{d}t\,\mathrm{d}x \tag{22}$$

Necessary conditions for optimality for a relative minimum of the cost function J require that its first variation be zero for any arbitrary admissible variation. As a result, we obtain the following adjoint equation and split boundary conditions:

$$\boldsymbol{\lambda}_t + (\mathbf{A}^T\boldsymbol{\lambda})_x + H_{1,\mathbf{y}}^T = \mathbf{0} \tag{23}$$

$$\mathbf{A}^T(\mathbf{y}(0,t),0)\boldsymbol{\lambda}(0,t) + H_{2,\mathbf{y}(0,t)}^T = \mathbf{0} \tag{24}$$

$$\mathbf{A}^T(\mathbf{y}(L,t),L)\boldsymbol{\lambda}(L,t) - H_{2,\mathbf{y}(L,t)}^T = \mathbf{0} \tag{25}$$

Upon simplification, the adjoint equation can be written as

$$\boldsymbol{\lambda}_t + (\mathbf{A}^T\boldsymbol{\lambda})_x - \mathbf{B}_{\mathbf{y}}^T\xi(x,v)\boldsymbol{\lambda} = \mathbf{0} \tag{26}$$

subject to the following boundary and terminal-time conditions:

$$(\mathbf{I} - \mathbf{F}^T)\mathbf{A}^T(\mathbf{y}(0,t),0)\boldsymbol{\lambda}(0,t) + \mathbf{F}^T\mathbf{A}^T(\mathbf{y}(L,t),L)\boldsymbol{\lambda}(L,t) = Q\mathbf{F}^T\mathbf{E}^T\mathbf{E}[\mathbf{y}(L,t) - \mathbf{y}_d(L)] \tag{27}$$

$$\boldsymbol{\lambda}(x,t_f) = \mathbf{0} \tag{28}$$

From the optimality conditions, we also obtain an optimal control for the air injection mass flow as

$$\int_0^{L}H_{1,v}\,\mathrm{d}x + H_{2,v} = 0 \tag{29}$$

Using the functional relationship in the parameter estimation, the optimal air injection mass flow control can be directly solved in terms of the adjoint vector $\boldsymbol{\lambda}(x,t)$

$$v = \mathrm{sat}(v_{\mathrm{opt}}) = \begin{cases} 0 & v \le 0 \\ v_{\mathrm{opt}} & 0 < v < v_{\mathrm{sat}} \\ v_{\mathrm{sat}} & v \ge v_{\mathrm{sat}} \end{cases} \tag{30}$$

where

$$v_{\mathrm{opt}} = v_d - \frac{\frac{2\Delta\xi_{\max}}{v_{\mathrm{sat}}}\left(1 - \frac{v_d}{v_{\mathrm{sat}}}\right)\int_0^{L}\boldsymbol{\lambda}^T\mathbf{B}\,\mathrm{d}x}{R - \frac{2\Delta\xi_{\max}}{v_{\mathrm{sat}}^2}\int_0^{L}\boldsymbol{\lambda}^T\mathbf{B}\,\mathrm{d}x} \tag{31}$$

To ensure a nonsingular optimal control solution, we require that

$$R \neq \frac{2\Delta\xi_{\max}}{v_{\mathrm{sat}}^2}\int_0^{L}\boldsymbol{\lambda}^T\mathbf{B}\,\mathrm{d}x \tag{32}$$

Because $\boldsymbol{\lambda}(x,t_f) = \mathbf{0}$, then the optimal control will converge to the desired air injection mass flow control as $t \to t_f$. We also want to ensure that the desired air injection mass flow control is not too close to the saturation value because the control will not be as effective beyond this value.

To compute the air injection control trajectory, we implement a second-order gradient method. First, we assume an initial but arbitrary control trajectory. Using this control, we proceed to solve a two-point boundary value problem involving the Euler equation and its adjoint using a wave-splitting, explicit-scheme, finite difference upwind method [13]. The new update on the control trajectory can then be computed from Eq. (31). The whole iterative process is repeated until a convergence on the control trajectory is achieved. This iterative gradient method results in a rapid convergence within two iterations due to the linear-quadratic cost function and the assumed quadratic relationship of the air injection mass flow control. Because of the fast convergence, the nonlinear trajectory optimization method can be adapted to a real-time computing of a desired air injection mass flow control trajectory.

The trajectory optimization solution generally provides an open-loop optimal control which can be used to command the air injection actuation. Using gain scheduling, the control can be turned into a feedback based on the trajectory of the desired total pressure at the outlet. In practice, the open-loop control is not robust enough because disturbances or modeling errors will immediately destroy the optimality of the control, thereby causing the output to not achieve a desired value. Therefore, an error-correction linearized feedback must be incorporated into the overall flow control architecture to deal with system disturbances and uncertainties resulting from a gas turbine engine operating environment.

VII. Error-Correction Linear Feedback Optimal Control

The objective of the error-correction feedback is to compensate for modeling errors or aerodynamic variation in the inlet flow condition which act as a disturbance to the flow through the stator cascade. The nonlinear trajectory optimization computes the values of the reference flow variables $\mathbf{y}(x,t)$ which are compared to the measured values. Error signals are then computed by subtracting the measured values from the reference values. Because the error signals should be small, the Euler equations can be linearized about the nominal control trajectory. The linear perturbation of the Euler equations is

$$\boldsymbol{\Delta}\,\mathbf{y}_t + \mathbf{A}\boldsymbol{\Delta}\mathbf{y}_x + \mathbf{A}\left[\mathbf{A}_{\mathbf{y}}^{-1}\mathbf{y}_t + (\mathbf{A}^{-1}\mathbf{B})_{\mathbf{y}}\xi(x,t)\right]\boldsymbol{\Delta}\mathbf{y} + \mathbf{B}\xi_v\Delta v = \mathbf{0} \tag{33}$$

We assume that the disturbances are manifested by changes in the inlet flow condition or modeling errors to cause the measured outputs to deviate from the reference trajectory. Because the mass flow and total temperature do not vary significantly through the stator cascade due to the conservation of mass and energy, we can make a reasonable assumption that their gradients are constant. Then the linearized momentum component of the Euler equations can be approximated as

$$a_1(x,t)\Delta p_{0,t} + \Delta p_{0,x} + a_2(x,t)\Delta p_0 + a_3(x,t)\Delta v + a_4(x,t)\Delta \dot{m}_i + a_5(x,t)\Delta T_{0,i} = 0 \tag{34}$$

subject to the boundary condition

$$\Delta p_0(0,t) = \Delta p_{0,i} \tag{35}$$

The coefficients in Eq. (34) are computed from $\dot{m}$, p_0, T_0, and M on the nominal trajectory as

$$a_1 = \frac{2+(\gamma-1)M^2}{4-2\gamma+(\gamma-1)M^2}\frac{1}{u} > 0$$

$$a_2 = -\frac{\gamma M^2(1+\gamma M^2)}{2(1-M^2)}\frac{\xi}{L}$$

$$a_3 = -\gamma p_0 M^2 \frac{\Delta\xi_{\max}}{L v_{\text{sat}}}\left(1-\frac{v}{v_{\text{sat}}}\right)$$

$$a_4 = \frac{\gamma p_0 M^2\left(1+\frac{\gamma-1}{2}M^2\right)}{\dot{m}(1-M^2)}\frac{\xi}{L}$$

$$a_5 = \frac{\gamma p_0 M^2\left(1+\frac{\gamma-1}{2}M^2\right)}{2T_0(1-M^2)}\frac{\xi}{L}$$

From Eq. (34), we see that changes in the inlet mass flow $\Delta\dot{m}_i$, total pressure $\Delta p_{0,i}$, and total temperature $\Delta T_{0,i}$ together act as disturbances to the total pressure error. The objective of the feedback control therefore is to regulate the total pressure error at the stator outlet under the influence of these disturbances. To compute the feedback control, we introduce a new quasi-steady state feedback optimal control approach based on the adjoint method. We contrast this approach with a standard linear-quadratic regulator (LQR) optimal control approach applied to a discretized form of Eq. (34) to illustrate the advantage of the proposed approach. To that end, we consider the following linear-quadratic cost function to minimize the total pressure error at the outlet and the corrective control action:

$$J = \int_0^{t_f}\left[\frac{1}{2}Q\Delta p_0^2(L,t) + \frac{1}{2}R\Delta v^2\right]\mathrm{d}t \tag{36}$$

where $Q \geq 0$ and $R > 0$.

The adjoint of the linearized Euler equation is

$$\lambda_t + \left(\frac{\lambda}{a_1}\right)_x - \frac{a_2\lambda}{a_1} = 0 \tag{37}$$

subject to the boundary condition:

$$\frac{\lambda(L,t)}{a_1(L,t)} = Q\Delta p_0(L,t) \tag{38}$$

The optimal control can be found as

$$R\Delta v - \int_0^L \frac{a_3\lambda}{a_1}\,\mathrm{d}x = 0 \tag{39}$$

We now assume an adjoint solution in the form of a linear combination of the total pressure error, the corrective control, and the mass flow and total temperature disturbances

$$\frac{\lambda(x,t)}{a_1(x,t)} = P_1(x,t)\Delta p_0(x,t) + P_2(x,t)\Delta v(t) + P_3(x,t)\Delta\dot{m}_i(t) + P_4(x,t)\Delta T_{0,i}(t) \tag{40}$$

Substituting this into Eqs. (37) and (38) and neglecting the term λ_t, which in essence gives rise to a quasi-steady state solution, yields

$$\frac{\partial}{\partial x}\begin{bmatrix}P_1\\P_2\\P_3\\P_4\end{bmatrix} = \begin{bmatrix}2a_2 & 0 & 0 & 0\\ a_3 & a_2 & 0 & 0\\ 0 & a_4 & a_2 & 0\\ 0 & 0 & a_5 & a_2\end{bmatrix}\begin{bmatrix}P_1\\P_2\\P_3\\P_4\end{bmatrix} \tag{41}$$

subject to the boundary conditions $P_1(L,t) = Q$, $P_{i\neq 1}(L,t) = 0$.

Similarly, we assume a solution for the linearized Euler equation of the form

$$\Delta p_0(x,t) = S_1(x,t)\Delta p_0(L,t) + S_2(x,t)\Delta v(t) + S_3(x,t)\Delta\dot{m}_i(t) + S_4(x,t)\Delta T_{0,i}(t) \tag{42}$$

Substituting this into Eq. (34) and again neglecting the term $\Delta p_{0,t}$ results in a quasi-steady state expression

$$\frac{\partial}{\partial x}\begin{bmatrix}S_1\\S_2\\S_3\\S_4\end{bmatrix} = -\begin{bmatrix}a_2 & 0 & 0 & 0\\ 0 & a_2 & 0 & 0\\ 0 & 0 & a_2 & 0\\ 0 & 0 & 0 & a_2\end{bmatrix}\begin{bmatrix}S_1\\S_2\\S_3\\S_4\end{bmatrix} - \begin{bmatrix}0\\a_3\\a_4\\a_5\end{bmatrix} \tag{43}$$

with the boundary conditions $S_1(L,t) = 1$, and $S_{i\neq 1}(L,t) = 0$.

Applying the boundary condition (35) and solving for Δv then yields

$$\Delta v(t) = \frac{1}{S_2(0,t)}[\Delta p_0(0,t) - S_1(0,t)\Delta p_0(L,t) - S_3(0,t)\Delta\dot{m}_i(t) - S_4(0,t)\Delta T_{0,i}(t)] \tag{44}$$

Substituting Eq. (44) back into Eq. (42) results in

$$\Delta p_0(x,t) = \left[S_1(x,t) - S_1(0,t)\frac{S_2(x,t)}{S_2(0,t)}\right]\Delta p_0(L,t) + \frac{S_2(x,t)}{S_2(0,t)}\Delta p_{0,i}(t) + \left[S_3(x,t) - S_3(0,t)\frac{S_2(x,t)}{S_2(0,t)}\right]\Delta\dot{m}_i(t) + \left[S_4(x,t) - S_4(0,t)\frac{S_2(x,t)}{S_2(0,t)}\right]\Delta T_{0,i}(t) \tag{45}$$

Upon substituting Eqs. (40) and (45) into the optimal control expression in Eq. (39), we obtain a feedback form for the air injection mass flow control as

$$\Delta v(t) = K_1(t)\Delta p_0(L,t) + K_2(t)\Delta p_{0,i}(t) + K_3(t)\Delta\dot{m}_i(t) + K_4(t)\Delta T_{0,i}(t) \tag{46}$$

where K_i, $i = 1,\ldots,4$ are the control gains defined as

$$K_1(t) = \frac{\int_0^L a_3(x,t)P_1(x,t)\left[S_1(x,t) - S_1(0,t)\frac{S_2(x,t)}{S_2(0,t)}\right]\mathrm{d}x}{R - \int_0^L a_3(x,t)P_2(x,t)\,\mathrm{d}x}$$

$$K_2(t) = \frac{\int_0^L a_3(x,t)P_1(x,t)\frac{S_2(x,t)}{S_2(0,t)}\,\mathrm{d}x}{R - \int_0^L a_3(x,t)P_2(x,t)\,\mathrm{d}x}$$

$$K_3(t) = \frac{\int_0^L a_3(x,t)\{P_1(x,t)\left[S_3(x,t) - S_3(0,t)\frac{S_2(x,t)}{S_2(0,t)}\right] + P_3(x,t)\}\,\mathrm{d}x}{R - \int_0^L a_3(x,t)P_2(x,t)\,\mathrm{d}x}$$

$$K_4(t) = \frac{\int_0^L a_3(x,t)\{P_1(x,t)\left[S_4(x,t) - S_4(0,t)\frac{S_2(x,t)}{S_2(0,t)}\right] + P_4(x,t)\}\,\mathrm{d}x}{R - \int_0^L a_3(x,t)P_2(x,t)\,\mathrm{d}x}$$

From Eq. (46), it can be seen that the error-correction feedback control only depends on the total pressure error at the outlet $\Delta p_0(L,t)$ as well as the disturbance inputs due to changes in the inlet condition of the stator cascade. The quasi-steady state control essentially transforms a control that depends on a total pressure error distribution along the stator cascade into one that only depends on the flow quantities at the stator inlet and outlet. Thus, it is a simpler type of feedback flow control as compared to a standard full-state feedback control scheme that requires all total pressure errors along the stator cascade to be measured or estimated such as the LQR optimal control method. Figure 8 illustrates a block diagram of the quasi-steady state error-correction feedback optimal control.

To contrast this quasi-steady state feedback control, we consider a standard error-correction feedback LQR optimal control for the flow control problem. First, to cast the linearized Euler equation into a standard state-space form, we discretize Eq. (33) into n discrete points along the stator cascade flow passage using a first-order upwind finite difference method. This results in

$$\dot{\mathbf{x}} = \mathbf{A}_e\mathbf{x} + \mathbf{B}_e\mathbf{u} + \mathbf{C}_e\mathbf{v} \tag{47}$$

where $\mathbf{x} = [\,\Delta p_{0,2} \quad \Delta p_{0,3} \quad \cdots \quad \Delta p_{0,n}\,]^T$ is the total pressure error vector, $\mathbf{u} = \Delta v$ is the corrective air injection mass flow control, $\mathbf{v} = [\,\Delta \dot{m}_i \quad \Delta p_{0,i} \quad \Delta T_{0,i}\,]^T$ is the inlet flow disturbance vector, and

$$\mathbf{A}_e = \begin{bmatrix} -\frac{1}{a_{1,1}\Delta x} & 0 & \cdots & 0 \\ \frac{1}{a_{1,2}\Delta x} - \frac{a_{2,2}}{a_{1,2}} & -\frac{1}{a_{1,2}\Delta x} & & 0 \\ \vdots & & \ddots & \vdots \\ 0 & \cdots & \frac{1}{a_{1,n-1}\Delta x} - \frac{a_{2,n-1}}{a_{1,n-1}} & -\frac{1}{a_{1,n-1}\Delta x} \end{bmatrix}$$

$$\mathbf{B}_e = \begin{bmatrix} -\frac{a_{3,1}}{a_{1,1}} \\ -\frac{a_{3,2}}{a_{1,2}} \\ \vdots \\ -\frac{a_{3,1}}{a_{1,1}} \end{bmatrix}, \qquad \mathbf{C}_e = \begin{bmatrix} -\frac{a_{4,1}}{a_{1,1}} & -\frac{a_{2,1}}{a_{1,1}} + \frac{1}{a_{1,1}\Delta x} & -\frac{a_{5,1}}{a_{1,1}} \\ -\frac{a_{4,2}}{a_{1,2}} & 0 & -\frac{a_{5,2}}{a_{1,2}} \\ \vdots & \vdots & \vdots \\ -\frac{a_{4,1}}{a_{1,1}} & 0 & -\frac{a_{5,1}}{a_{1,1}} \end{bmatrix}$$

We note that $\Delta p_{0,j} = \Delta p_0(x_j,t)$, and $a_{i,j} = a_i(x_j,t)$. To have a better regulation performance, we will incorporate an integral compensator for the total pressure error at the outlet into the design. The state-space form is now augmented with the additional integral error as

$$\begin{bmatrix} \dot{\mathbf{x}}_1 \\ \dot{\mathbf{x}}_2 \\ \dot{z} \end{bmatrix} = \begin{bmatrix} \mathbf{A}_{e,11} & \mathbf{0} & \mathbf{0} \\ \mathbf{A}_{e,21} & \mathbf{A}_{e,22} & \mathbf{0} \\ \mathbf{0} & \mathbf{D}_e & 0 \end{bmatrix} \begin{bmatrix} \mathbf{x}_1 \\ \mathbf{x}_2 \\ z \end{bmatrix} + \begin{bmatrix} \mathbf{0} \\ \mathbf{B}_{e,2} \\ 0 \end{bmatrix} \mathbf{u} + \begin{bmatrix} \mathbf{C}_{e,1} \\ \mathbf{C}_{e,2} \\ 0 \end{bmatrix} \mathbf{v} \tag{48}$$

where $\mathbf{x}_1 = [\,\Delta p_{0,2} \quad \Delta p_{0,3} \quad \cdots \quad \Delta p_{0,m}\,]^T$ are the noncontrollable total pressure errors because they are located upstream of the location of the air injection $\mathbf{x}_{m+1}$, $\mathbf{x}_2 = [\,\Delta p_{0,m+1} \quad \Delta p_{0,m+2} \quad \cdots \quad \Delta p_{0,n}\,]^T$ are the controllable total pressure errors, $z = \int_0^{t_f} \Delta p_{0,n}\,\mathrm{d}t$ is the integral error of the total pressure at the outlet, $\mathbf{A}_{e,ij}$, $\mathbf{B}_{e,i}$, $\mathbf{C}_{e,i}$ are appropriate partitioned matrices, and $\mathbf{D}_e = [\,0 \quad 0 \quad \cdots \quad 1\,]$.

Because $\mathbf{x}_1$ is uncoupled from $\mathbf{x}_2$ and the control $\mathbf{u}$, it can be computed directly from

$$\dot{\mathbf{x}}_1 = \mathbf{A}_{e,11}\mathbf{x}_1 + \mathbf{C}_{e,1}\mathbf{v} \tag{49}$$

Then the controllable state-space equation becomes

$$\dot{\mathbf{z}} = \bar{\mathbf{A}}_e\mathbf{z} + \bar{\mathbf{B}}_e\mathbf{u} + \mathbf{w} \tag{50}$$

where $\mathbf{z} = [\,\mathbf{x}_2 \quad z\,]^T$ is the integral-compensated state vector, $\mathbf{w} = [\,\mathbf{C}_{e,2}\mathbf{v} + \mathbf{A}_{e,21}\mathbf{x}_1 \quad 0\,]^T$ is the disturbance vector at the location of the air injection, and

$$\bar{\mathbf{A}}_e = \begin{bmatrix} \mathbf{A}_{e,22} & \mathbf{0} \\ \mathbf{D}_e & 0 \end{bmatrix}$$

The discretized flow model of the stator cascade is now in a standard controllable state-space form that can be used for an LQR design. The optimal feedback air injection mass flow control can be found as a full-state feedback and a disturbance feedforward as

$$\mathbf{u} = -\mathbf{R}^{-1}\bar{\mathbf{B}}_e^T(\mathbf{W}\mathbf{z} + \mathbf{V}\mathbf{w}) \tag{51}$$

where $\mathbf{W}$ and $\mathbf{V}$ are the solutions to the algebraic Riccati equations with weighting matrices $\mathbf{Q} \geq 0$ and $\mathbf{R} > 0$ [18]

$$\bar{\mathbf{A}}_e^T\mathbf{W} + \mathbf{W}\bar{\mathbf{A}}_e - \mathbf{W}\bar{\mathbf{B}}_e\mathbf{R}^{-1}\bar{\mathbf{B}}_e^T\mathbf{W} + \mathbf{Q} = \mathbf{0} \tag{52}$$

$$\mathbf{V} = \left(\mathbf{W}\bar{\mathbf{B}}_e\mathbf{R}^{-1}\bar{\mathbf{B}}_e^T - \bar{\mathbf{A}}_e^T\right)\mathbf{W} \tag{53}$$

Typically with the full-state feedback LQR approach, we would need to include a reduced-order or full-state observer to estimate all the total pressure error along the cascade flow passage based on the measurements at the inlet and the outlet of the stator cascade. This would then add an additional degree of complexity to the LQR feedback control method. The LQR feedback scheme is illustrated in Fig. 9.

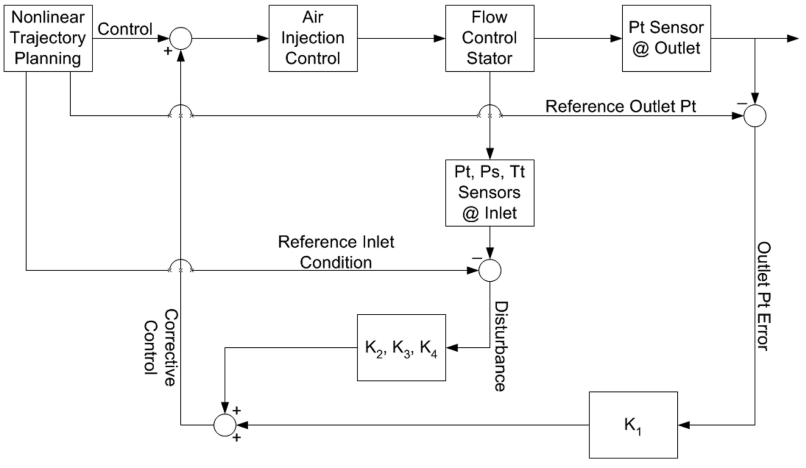

Fig. 8 Quasi-steady state feedback block diagram.

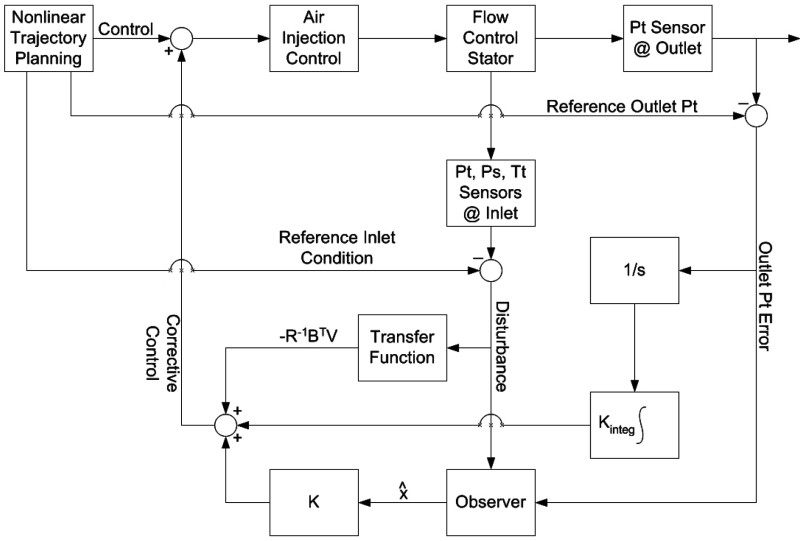

Fig. 9 LQR feedback block diagram.

Contrasting the quasi-steady state feedback control and the standard LQR control, we see that the quasi-steady state feedback control affords a number of advantages over the LQR method in that it does not require estimation of the total pressure error distribution nor does it require solving a full-state Riccati equation. Because the quasi-steady state feedback uses the measured flow quantities at the inlet and the outlet for feedback, it should, in principle, provide a more robust control than the LQR approach.

VIII. Results and Discussion

To demonstrate the flow control architecture, a flow control simulation is performed. A representative midradius stator cascade is selected for the study. The notional stator blade has a NACA 65-series low-speed profile, a camber angle of 30 deg, a stagger angle of 45 deg, and a solidity of 1, which is comparable to the LSAC flow control vane. The inlet condition is specified to be at a mass flow of 0.0222 slug/s, a total pressure of 2116.2 psf, and a total temperature of 529.67°R. Based on the resulting flow passage, an area distribution per unit length of the 2-D cascade duct along the midstreamline is computed as shown in Fig. 10.

Figure 10 reveals that the flow passage area decreases near the leading edge, thus indicating an accelerating flow as expected. The flow passage then opens up, forming a diffuser and thereby causing the flow to decelerate that consequently results in a static pressure recovery from the kinetic energy of the flow. It is the adverse pressure gradient in a diffusing flow passage that tends to promote flow separation.

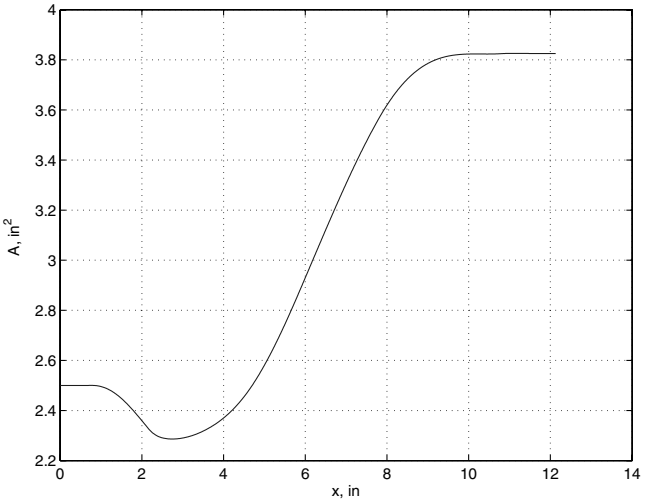

Fig. 10 Area distribution of cascade flow passage.

To model the stator cascade based on the 1-D unsteady Euler equations, the 2-D cascade duct is discretized into a finite number of computing stations that capture reasonably well the cascade geometry. A time step of 0.02 ms is selected so as to satisfy the Courant–Friedrichs–Levy (CFL) stability condition [13], assuming that the flow remains subsonic throughout the flow passage. Applying the Nyquist frequency criterion, the frequency range of interest would be 25 kHz, which is adequate to address the frequency requirement of 10 kHz for actuation. Thus, using the time-accurate 1-D unsteady flow equations for flow control modeling would ensure that the high-frequency requirement could be met.

An arbitrary inlet air angle of 60 deg is selected. This air inlet angle results in an angle of attack of 15 deg. The performance of this cascade is then predicted by the NACA 65-series cascade correlation method based on the Carter's rule correlation method

$$\Delta\beta = \beta_1 - \beta_2 = i_0 - \delta_0^0 + \theta(1 - m + n) \tag{54}$$

where $\Delta\beta$ is the turning angle, i_0 is the reference minimum-loss incidence angle, δ_0^0 is the reference deviation angle at the reference incidence angle, θ is the blade camber angle, and m and n are the slope parameters as functions of the air inlet angle β_1 and the solidity σ [8].

Carter's rule predicts an outlet air angle of 40 deg or a 20 deg turning angle. The difference of 10 deg from the blade camber angle is the flow deviation angle which is due to flow separation that normally occurs on the suction surface. The diffusion factor for this cascade as computed from Eq. (3) is 0.6078 which exceeds a recommended maximum diffusion factor of 0.55 for stall free operation and corresponds to a total pressure loss coefficient of 0.1910. To reduce the tendency for flow separation, we would like to reduce the diffusion factor to about 0.5, which correspond to a total pressure loss coefficient of 0.1228. So, we would like to seek a total pressure set point of 2060.1 psf or an air injection mass flow of 1.1104×10^{-4} slug/s which is about 0.5% of the total mass flow. The optimal control trajectory as computed from the nonlinear trajectory planning is shown in Fig. 11a.

The nonlinear trajectory optimization is solved using a second-order gradient method. To start the solution process, a step input for the air injection control is used. The weighting factors $Q = 1 \times 10^{-5}$ and $R = 1 \times 10^{8}$ for the cost function are selected. The computation converges rapidly to the optimal solution within two iterations. The air injection mass flow time history shows an initial modulation before quickly settling to the desired air injection mass flow. Figure 11b shows the total pressure response at the outlet lagging the air injection mass flow control by a small time delay as a result of the fluid transport propagation. Figure 12 illustrates an optimal trajectory of the gain schedule as a function of the total pressure error from the set point at the outlet. The gain schedule allows the air injection mass

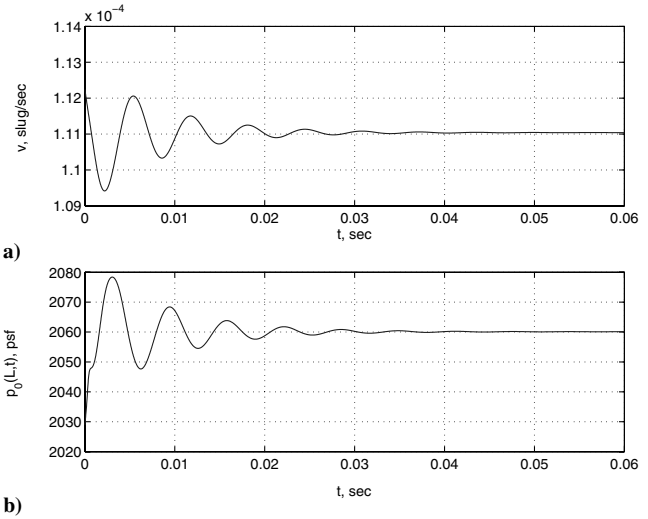

Fig. 11 a) Nonlinear optimal air injection control and b) total pressure response at outlet.

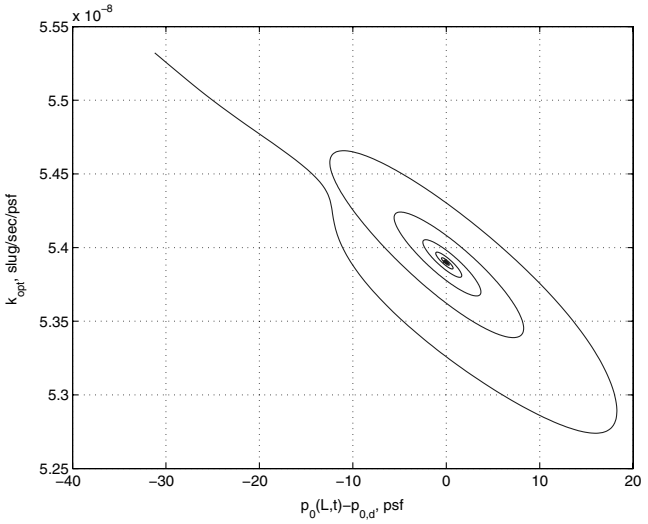

Fig. 12 Gain schedule.

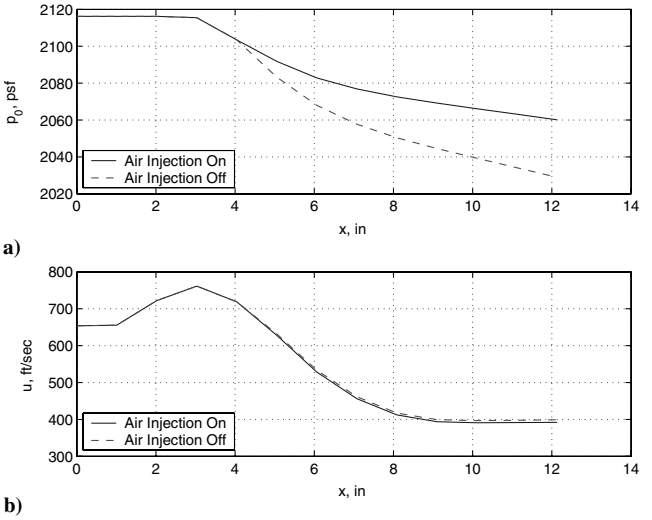

Fig. 13 a) Total pressure distribution and b) velocity distribution.

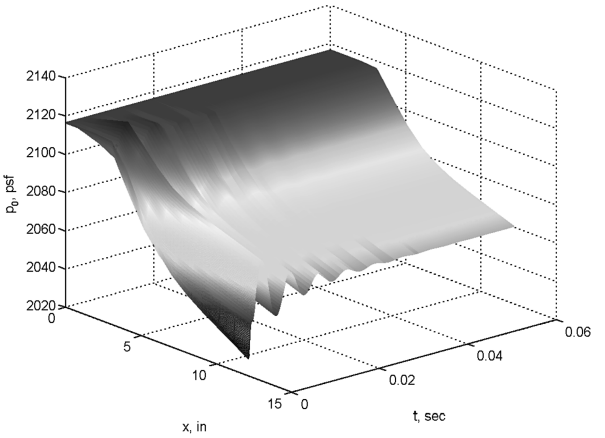

Fig. 14 Total pressure response surface.

flow control to be computed as follows:

$$v(t) = v_d + K_{\text{opt}}[p_0(L,t) - p_{0,d}(L)] + K_{\text{opt}}p_{0,d}(L) \qquad (55)$$

Figure 13a shows the total pressure distribution along the cascade flow passage with the air injection control on and off. It is noted that near the leading edge, the flow is modeled as loss free because of the convergent flow passage, wherein the boundary layer is thinned resulting from a favorable pressure gradient associated with an accelerating flow as seen in Fig. 13b. At the point of maximum velocity, the total pressure rapidly decreases due to the boundary layer thickening in the divergent flow passage. With the air injection control on, the total pressure at the outlet is raised above that with no air injection control. The total pressure distribution as computed by the Euler equations is also plotted as a surface function of space and time in Fig. 14. The velocity distributions as shown in Fig. 13b are similar with and without air injection control. The outlet velocity with no air injection control is slightly higher than that with the air injection control as expected. Without the air injection control, the outlet tangential velocity component should be higher, corresponding to a lower air turning angle, than it would be if the air injection control is on that would result in an improved air turning capability of the stator cascade.

The air injection control history computed from the nonlinear trajectory optimization is normally used as an open-loop control. In practice, changes in the aerodynamic condition at the stator inlet may result in a discrepancy between the model prediction and the behavior of the actual flowfield. These aerodynamic changes act as disturbances to the flow control system. If left uncorrected, the total pressure at the stator outlet will not achieve its desired set point. Thus, it is necessary to incorporate an error-correction feedback control.

To demonstrate the error-correction feedback control, we synthesize a variation in the inlet flow condition that results in a mass flow perturbation of 1.2163×10^{-4} slug/s, a total pressure perturbation of 10.6 psf, and a total temperature perturbation of 2.68°R. The error-correction feedback control is computed using both the quasi-steady state and the LQR approaches. For the quasi-steady state method, we select weighting factors $Q = 1 \times 10^{-2}$ and $R = 1$. The optimal quasi-steady state feedback gains are plotted in Fig. 15. The optimal feedback corrective air injection mass flow control is plotted in Fig. 16a and the resulting total pressure error response is plotted in Fig. 16b. We note that the total pressure error does not quite reach zero as the control incurs a very small steady-state error. This steady-state error is due to the lack of an integrator in the feedback control. A future implementation of a quasi-steady state feedback control with an integrator will be considered.

Next, we consider the LQR design with weighting matrices $\mathbf{Q} = 1 \times 10^{-4}\mathbf{I}$ and $R = 1 \times 10^{8}$. The LQR corrective air injection mass flow control is obtained as shown in Fig. 17a. The corresponding total pressure error response at the outlet is plotted in Fig. 17b.

Comparing Figs. 16 and 17 between the quasi-steady state control and the LQR control, we see that the LQR method results in the total pressure error at the stator outlet converging to zero due to the presence of the integrator. The disadvantage of the LQR method lies in its complexity because the feedback control requires an observer design which is not included in this study. As can be seen, for the

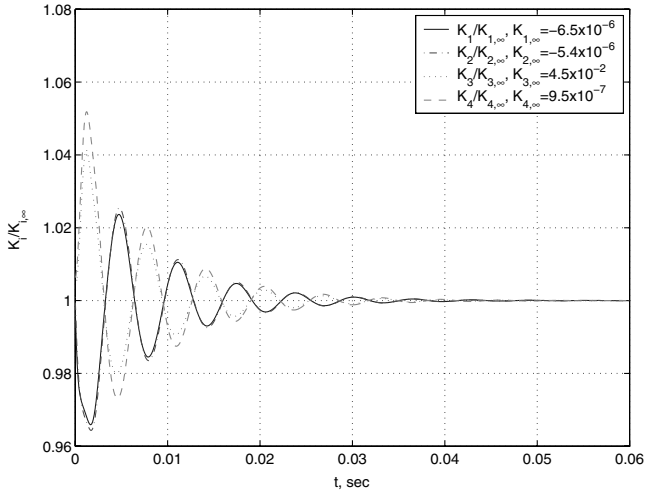

Fig. 15 Quasi-steady state feedback gain ratios.

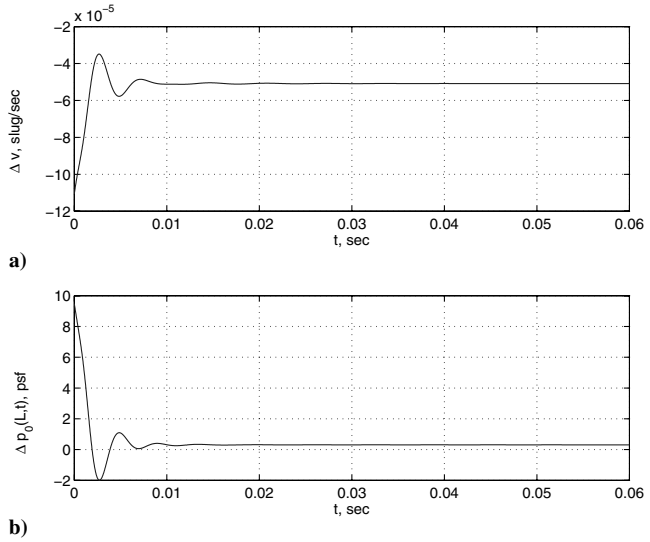

Fig. 16 a) Quasi-steady state corrective air injection mass flow control and b) total pressure error response at outlet.

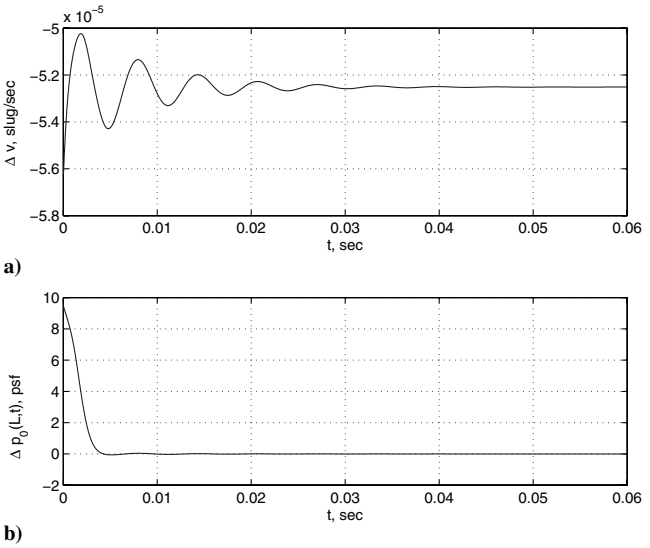

Fig. 17 a) LQR corrective air injection mass flow control and b) total pressure error response at outlet.

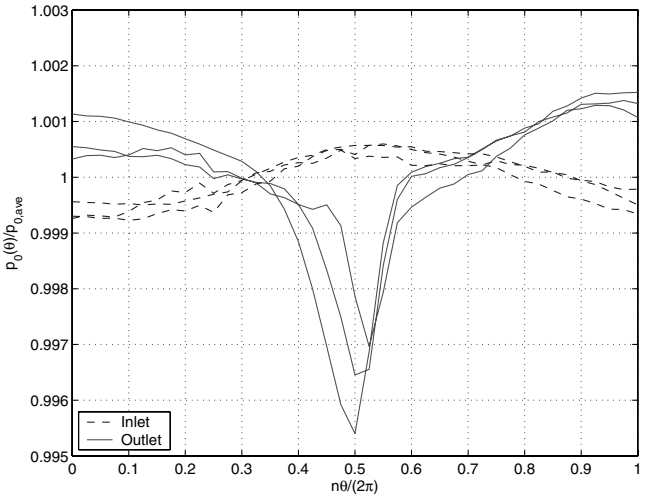

Fig. 18 Tangential variations of total pressure at stator inlet and outlet.

quasi-steady state method, the error-correction feedback control is quite effective even though there exists a small steady-state error.

It should be noted that in the present flow control method, we have not considered the effects of dynamics of the air injection mass flow control valve and line loss in the pressure tubing. In practice, these effects can potentially limit the overall performance of the flow control design. Typically, flow control valves tend to have longer time constants than the fluid transport time. As a result, the actual response of the air injection mass flow is likely slower than the computed trajectory. However, the steady-state value of the air injection mass flow should still be achievable if the flow control valve has a sufficient range. Thus, to improve the frequency response of the flow control, a flow control valve with a desirable frequency performance should be selected. The effect of line loss in the pressure tubing is generally more adverse than the dynamics of the flow control valve. If the pressure tubing line from the bleed air reservoir is significantly long, the mass flow will likely be throttled down due to the line loss effect. This would potentially result in an underactuated control whereby the flow control valve would not be able to deliver the correct air injection mass flow. Moreover, the line loss effect also causes a time delay in the delivery of the air injection mass flow. Therefore, it is important that the pressure tubing line be kept as short as possible to maintain a proper performance of the flow control.

The issue of sensor placements is critical in designing an effective flow control. Real flow in a compressor cascade exhibits a tangential variation. Because the pressure loss parameter is determined from the tangentially average total pressure quantities, the cascade flow passage at the inlet and the outlet should be covered sufficiently with total pressure sensors. Alternatively, a single sensor could be placed at a strategic location that allows it to measure a local total pressure quantity that is approximately equal to the tangentially average total pressure quantity. Figure 18 shows a sample of three tangential variations of the total pressure measurements normalized to the flow-weighted tangentially average total pressure at the stator inlet and outlet. The abscissa $n\theta/2\pi$ is the tangential coordinate of the flow passage around one stator blade with $0 \leq n\theta/2\pi < \frac{1}{2}$ being the flow region below the pressure surface. As can be seen, the total pressure at the outlet exhibits a sharp wake at the trailing edge. Based on these total pressure profiles, it appears that a single total pressure sensor could be placed at $n\theta/2\pi \approx 0.32$ at the inlet and the outlet where the local total pressure is about equal to the average total pressure.

IX. Conclusions

This paper has presented a flow control method using air injection as a means for flow separation control in a compressor stator cascade. The flow control is based on a fluid–physics model using the 1-D unsteady Euler equations with a total pressure loss parameter that represents the viscous dissipation associated with flow separation in a compressor cascade. The total pressure loss parameter is estimated using a recursive least-square parameter estimation process based on a quadratic relationship that describes the effect of the air injection

mass flow control on the total pressure loss reduction. A derivation of the adjoint equations for optimality of the 1-D Euler equations is presented. A nonlinear optimal control trajectory planning is designed based on an adjoint method for a hyperbolic equation. A second-order gradient has been implemented to provide a rapid computation of the optimal trajectory from which a gain schedule can be determined to enable the air injection control to achieve a desired total pressure set point at the outlet. A new quasi-steady state error-correction feedback method has been introduced. This method has been demonstrated to provide an effective error-correction feedback control using only the total pressure output without needing an observer as required by a standard LQR approach.

Acknowledgment

The authors would like to thank Carolyn Mercer, manager of the Intelligent Propulsion Systems Foundation Technology project at NASA Glenn Research Center, for the funding support of this work.

References

[1] Lord, W. K., MacMartin, D. G., and Tillman, T. G., "Flow Control Opportunities in Gas Turbine Engines," AIAA Paper 2000-2234, June 2000.

[2] MacMartin, D. G., Murray, R. M., Verma, A., and Paduano, J. D., "Active Control of Integrated Inlet/Compression Systems: Initial Results," FEDSM Paper 2001-18275, June 2001.

[3] Leinhos, D. C., Scheidler, S. G., and Fottner, L., "Experiments in Active Stall Control of a Twin-Spool Turbofan Engine," GT Paper 2002-30002, June 2002.

[4] d'Andrea, R., Behnken, R. L., and Murray, R. M., "Active Control of an Axial Flow Compressor via Pulsed Air Injection," California Institute of Technology CDS, Rept. 95-029, July 1996.

[5] Culley, D. E., Bright, M. M., Prahst, P. S., and Strazisar, A. J., "Active Flow Separation Control of a Stator Vane Using Surface Injection in a Multistage Compressor Experiment," GT Paper 2003-38863, June 2003.

[6] Moore, F. K., and Greitzer, E. M., "A Theory of Post-Stall Transients in Axial Compression Systems: Part 1 Development of Equations," *Journal of Engineering for Gas Turbines and Power*, Vol. 108, Jan. 1986, pp. 972–973.

[7] Blevins, R. D., *Applied Fluid Dynamics Handbook*, Van Nostrand Company, New York, 1984.

[8] National Aeronautics and Space Administration, *Aerodynamic Design of Axial-Flow Compressors*, NASA SP-36, 1965.

[9] Dixon, S. L., *Fluid Mechanics—Thermodynamics of Turbomachinery*, 3rd ed., Pergamon Press, New York, 1989.

[10] Ravindran, S. S., "Reduced-Order Adaptive Controllers for Fluid Flows Using POD," *Journal of Scientific Computing*, Vol. 15, No. 4, 2000, pp. 457–478.

[11] Shapiro, A. H., *The Dynamics and Thermodynamics of Compressible Fluid Flow*, Vol. 2, Ronald Press Company, New York, 1954.

[12] Stengel, R. F., *Optimal Control and Estimation*, Dover Publications, Inc., New York, 1994.

[13] Hirsh, C., *Numerical Computation of Internal and External Flows*, Vol. 1, Wiley, Brussels, 1991.

[14] Becker, R., Kapp, H., and Rannacher, R., "Adaptive Finite Element Methods for Optimal Control of Partial Differential Equations: Basic Concept," *SIAM Journal on Control and Optimization*, Vol. 39, No. 1, 2000, pp. 113–132.

[15] Jameson, A., Pierce, N., and Martinelli, L., "Optimum Aerodynamic Design Using the Navier-Stokes Equations," *Theoretical Computational Fluid Dynamics*, Vol. 10, Nos. 1–4, 1998, pp. 213–237.

[16] Nadarajah, S., and Jameson, A., "A Comparison of The Continuous and Discrete Adjoint Approach to Automatic Aerodynamic Optimization," AIAA Paper 2000-0667, Jan. 2000.

[17] Nguyen, N., and Ardema, M., "Optimal Control of Flow Recirculation in a Wind Tunnel," AIAA Paper 2004-4759, Aug. 2004.

[18] Brogan, W. L., *Modern Control Theory*, 3rd ed., Prentice–Hall, Upper Saddle River, NJ, 1991.

K. Ghia
Associate Editor